ACS OMEGA

http://pubs.acs.org/journal/acsodf

Article

Detection of Membrane Potential-Dependent Rhodopsin Fluorescence Using Low-Intensity Light Emitting Diode for Long-Term Imaging

Shiho Kawanishi, Keiichi Kojima,* Atsushi Shibukawa, Masayuki Sakamoto, and Yuki Sudo*

Cite This: *ACS Omega* 2023, 8, 4826−4834

Read Online

ACCESS | Metrics & More | Article Recommendations | Supporting Information

ABSTRACT: Microbial rhodopsin is a family of photoreceptive membrane proteins that commonly consist of a seven-transmembrane domain and a derivative of vitamin-A, retinal, as a chromophore. In 2011, archaeorhodopsin-3 (AR3) was shown to exhibit voltage-dependent fluorescence changes in mammalian cells. Since then, AR3 and its variants have been used as genetically encoded voltage indicators, in which mostly intense laser stimulation (1−1000 W/cm^2) is used for the detection of dim fluorescence of rhodopsin, leading to high spatiotemporal resolution. However, intense laser stimulation potentially causes serious cell damage, particularly during long-term imaging over minutes. In this study, we present the successful detection of voltage-sensitive fluorescence of AR3 and its high fluorescence mutant Archon1 in a variety of mammalian cell lines using low-intensity light emitting diode stimulation (0.15 W/cm^2) with long exposure time (500 ms). The detection system enables real-time imaging of drug-induced slow changes in voltage within the cells for minutes harmlessly and without fluorescence bleaching. Therefore, we demonstrate a method to quantitatively understand the dynamics of slow changes in membrane voltage on long time scales.

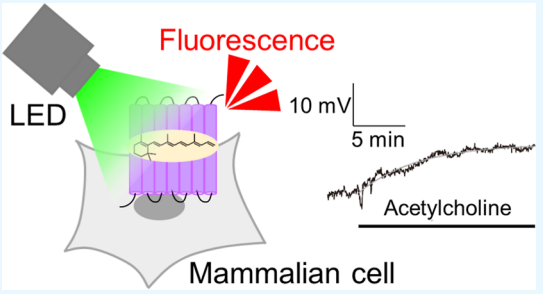

INTRODUCTION

Microbial rhodopsin is a family of photoreceptive membrane proteins that play central roles in photoreception in microorganisms.[1−3] Rhodopsin proteins commonly consist of a seven-transmembrane domain and a derivative of vitamin-A, retinal, as a chromophore (Figure 1a).[1−3] Retinal is covalently bound to a conserved lysine residue of the apoprotein (called opsin) through a protonated Schiff base linkage. Light absorption by rhodopsin causes bond-selective isomerization of retinal from all-trans to 13-cis forms within femtoseconds.[1] After photoisomerization, rhodopsins form several kinetically distinctive photointermediates (e.g., K-, L-, M-, N-, and O-intermediates) that exhibit different spectral sensitivities and then return to the initial state through reisomerization (Figure 1b). During the cyclic reaction called the photocycle, rhodopsins exhibit cognate molecular functions, such as ion pump, ion channel, phototactic sensor, and enzymes, leading to cellular responses.[1−3]

In 2011, archaeorhodopsin-3 (AR3 or Arch), a rhodopsin molecule identified as an outward proton pump in the extreme halophilic archaeon *Halobacterium sodomense*, was shown to exhibit voltage-dependent fluorescence changes in mammalian cells (Figure 1a).[4,5] The unique characteristics allowed us to use AR3 as a genetically encoded voltage indicator (GEVI).[6] Since then, several AR3 variants (e.g., QuasAr1, QuasAr2, Archon1, Archon2, paQuasAr3, NovArch, and QuasAr6) have been progressively produced by random mutagenesis to improve their fluorescence yield, signal-to-noise ratio, membrane localization, and response kinetics.[7−11] In contrast to other conventional methods to detect membrane voltage (i.e., electrodes and membrane voltage-sensitive dyes), microbial rhodopsin-based GEVIs have the following features:[6,12,13] (i) they can be accurately targeted for specific cells using genetic methods; (ii) they can noninvasively image individual cells; (iii) they can directly visualize membrane voltage on a millisecond time scale. Because of these features, the rhodopsin-based GEVIs have been attracting attention as an excellent tool for voltage imaging mainly in neurons.[4,6−9,14] In contrast, the rhodopsin-based GEVIs exhibit lower fluorescence intensities (FIs) than the enhanced green fluorescence protein (EGFP) (1/10−1/500).[4,15] Spectroscopic studies have shown that the fluorescence is emitted from the fluorescent photointermediate named Q-intermediate in AR3 (Figure 1b).[15,16] Since the Q-intermediate is formed by photon absorption from the precursor N-intermediate, three-photon excitation to the initial state (the first photon to the initial state, second to the N-intermediate, and third to the Q-

Received: October 30, 2022
Accepted: January 13, 2023
Published: January 25, 2023

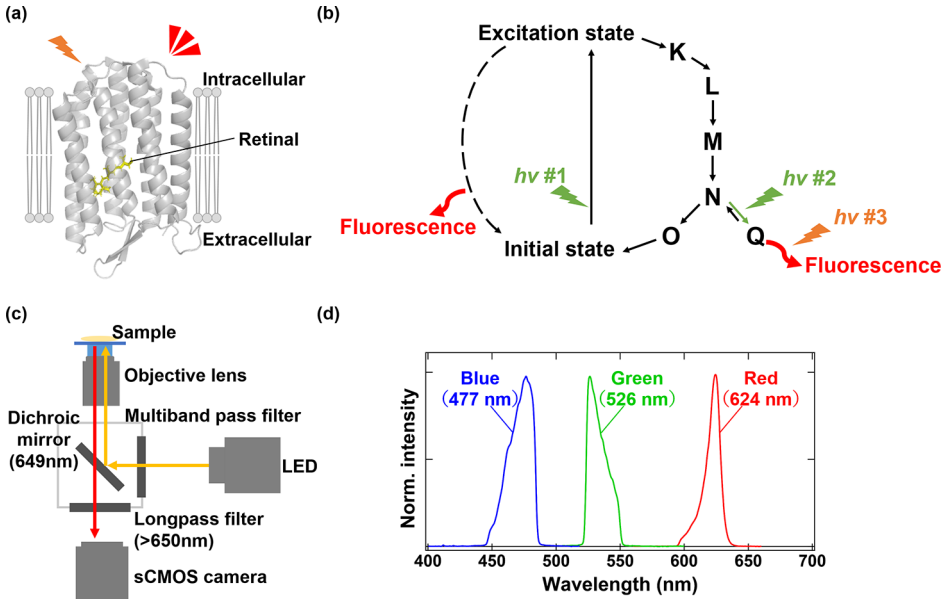

Figure 1. Archaerhodopsin-3 (AR3) as a fluorescence protein and its detection system with an LED. (a) Crystal structure of AR3 (PDB code: 6GUZ). AR3 shows near-infrared fluorescence. (b) Photoreaction scheme of microbial rhodopsins. After absorbing photons at the initial state, rhodopsins form several spectroscopically distinctive photointermediates (K-, L-, M-, N-, and O-intermediates) and then return to the initial state. Fluorescence is emitted from the Q-intermediate that is formed by photon absorption from the precursor N-intermediate, and the signal intensity highly depends on the membrane voltage in AR3. The voltage-dependent fluorescence is proposed to be emitted from the excited state for AR3 variants, such as QuasAr2 and Archon1. (c) Inverted microscopic setup for detecting rhodopsin fluorescence. LED light was passed through a multiband pass filter and an objective lens to stimulate the cell samples. The light intensity was adjusted to 0.15 W/cm^2. The NIR fluorescence images through a dichroic mirror and a long-pass filter (>650 nm) were obtained using an sCMOS camera. (d) Spectra of blue, green, and red LEDs through a multiband pass filter normalized at peak intensities. Peak wavelengths were 477 (blue), 526 (green), and 624 nm (red).

intermediate) is required for fluorescence emission. On the other hand, it has been proposed that the fluorescence is emitted from the excited state for AR3 variants, such as QuasAr2 and Archon1 (Figure 1b).[7,17] To overcome the low FI, intense laser stimulation (1−1000 W/cm^2) is used to realize voltage imaging of neurons (particularly the action potential) with high temporal resolution (approximately 500 μs).[4,6−9,14]

High-intensity laser stimulation has toxic and lethal effects on irradiated cells and tissues, specifically for long-term stimulation.[18] For instance, intense laser stimulation induces a decrease in viability and proliferation of human skin fibroblast cells[19] and causes the release of the toxic molecule such as nitric oxide in macrophages.[20] Moreover, intense laser stimulation causes intense heating of cells, leading to changes in cellular activities and cell damage.[18,21] Since many voltage imaging experiments using high-intensity laser lasts only for 30 s or less,[4,7,8] we speculate that the existing system with high-intensity lasers induces undesired damage to target cells, specifically for the long-term experiments over minutes. Compared to the fast voltage changes (e.g., neural action potential), living cells exhibit relatively slow voltage changes via intracellular signal transduction cascades (e.g., heterotrimeric G protein signaling, Ca^{2+} responses, and ATP production) and osmotic changes.[22−25] The slow changes are involved in various natural cellular responses and related diseases (e.g., contractile and endocrine responses, proliferation, and homeostasis).[26−28] However, the existing high-intensity laser-based imaging systems have not been applied for the real-time detection of slow changes in voltage, probably owing to cell damage. In addition, the high cost and significant effort required for laser systems compared to those of easy-to-use light sources [e.g., light emitting diode (LED) and halogen lamps] are the major limitations in expanding the application of rhodopsin-based GEVIs in the field of life sciences. Therefore, a low-intensity LED can be suitable as a light source to detect slow changes in voltage using rhodopsin-based GEVIs with low cost and effort.

In this study, we developed a new imaging system for rhodopsin-based GEVIs using a low-intensity LED as a light source (0.15 W/cm^2). Using this system, we successfully detected the voltage-sensitive fluorescence of AR3 and its high fluorescent mutant Archon1 in different mammalian cell lines with an exposure time of 500 ms. Of note, the detection system allowed real-time imaging of drug-induced slow changes in the voltage of mammalian cells for 20 min harmlessly and without fluorescence bleaching. Based on the results, we discuss the potential of combining rhodopsin-based GEVIs and low-intensity LEDs for the long-term imaging of slow dynamics of membrane voltage.

RESULTS AND DISCUSSION

Detection of AR3- and Archon1-Mediated Fluorescence Using Low-Intensity LED in HEK293 Cells. To realize the imaging of rhodopsin fluorescence with low-intensity light sources, we constructed an LED-based detection system using an inverted microscope (Figure 1c). Red, green, and blue LEDs were used as stimulus light sources. LED light was passed through a multiband pass filter and an objective lens to provide stimulus light to cultured cells. The peak wavelengths of the stimulus light are 624, 526, and 477 nm for red, green, and blue LED light sources, respectively (Figure 1d). To efficiently collect the fluorescence signals, we employed an oil immersion objective lens (100×/1.3 NA)

https://doi.org/10.1021/acsomega.2c06980
ACS Omega 2023, 8, 4826−4834

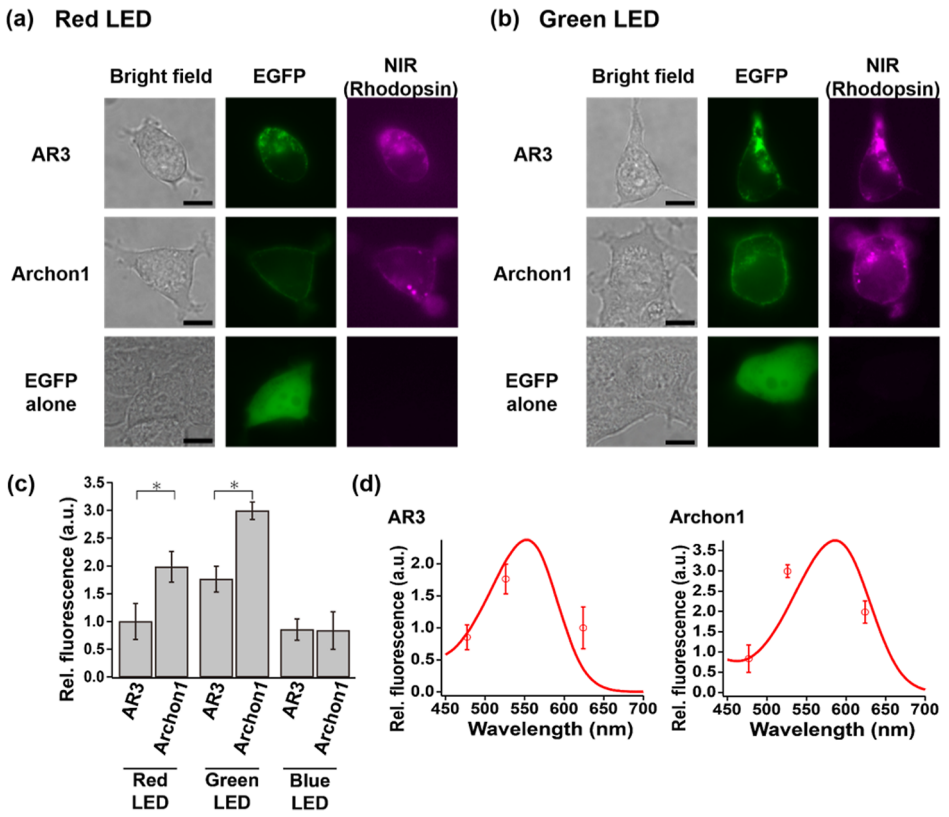

Figure 2. Fluorescence of AR3 and Archon1 in HEK293 cells. (a,b) Bright field and fluorescence images of HEK293 cells expressing AR3-EGFP (AR3), Archon1-EGFP (Archon1), and EGFP alone. The EGFP fluorescence images were obtained with excitation at 460−495 nm and emission over 510 nm, and NIR fluorescence images of rhodopsin were obtained with red (a) and green (b) LED stimulation. The NIR fluorescence signals were collected at a spectral range over 650 nm. Bright field images of the cells are also shown. The images were acquired with the oil immersion objective lens (100×/1.3 NA). All scale bars represent 10 μm. (c) Comparison of rhodopsin FIs between AR3 and Archon1 with red, green, and blue LED stimulation. In the target cells, plasma membrane regions were selected, and the integrated intensities of rhodopsin fluorescence signals were measured. Then, the FIs were normalized by the FI of AR3 with red LED excitation to obtain the relative FIs shown in panel (c,d). The data are shown as means ± the standard error of means (SEM) (n = 3−8 cells). Asterisks (*) indicate significant differences between the values (p < 0.05; Student's t-test, two-tailed). (d) Wavelength dependence of rhodopsin FIs of AR3 (left panel) and Archon1 (right panel). Absorption spectra of purified AR3 and Archon1 were overlayed. The data are shown as means ± SEM (n = 3−8 cells).

and an sCMOS camera (Figure 1c). Since rhodopsins exhibit near-infrared (NIR) fluorescence (around 660−760 nm),[16] we only collected NIR fluorescence signals using a long-pass filter (>650 nm) and imaged it on the sCMOS camera.

Here, we sought to detect NIR fluorescence in mammalian HEK293 cells, which have been widely used for rhodopsin expression,[8,29,30] with the above microscopic setup. As rhodopsin-based GEVIs, we tested wild-type AR3 and its high fluorescence mutant Archon1. According to our previous study,[15] the rhodopsin genes were fused with the EGFP gene as an expression marker, and the fused genes were inserted downstream of the mammalian CAG promoter (Figure S1a). In addition, a trafficking signal motif and an endoplasmic reticulum export motif were fused with the rhodopsin-EGFP construct to enhance their membrane localization in mammalian cells. When we imaged the transfected cells, the fluorescence signals of EGFP surrounding the plasma membrane of the cells were observed as previously described,[15] implying the successful expression of AR3 and Archon1 in HEK293 cells. Then, we imaged rhodopsin-EGFP-expressing cells with red LED stimulation (624 nm) since red laser stimulation (around 620 nm) is generally used to detect rhodopsin fluorescence.[4,7,14] At the light intensity of 0.15 W/cm^2 and an exposure time of 500 ms, we detected NIR fluorescence signals for AR3-EGFP- and Archon1-EGFP-expressing cells, which were mainly distributed in the plasma membrane (Figure 2a). In contrast, the NIR signals were hardly observed for EGFP-expressing cells with the same procedure (Figure 2a). NIR FIs were normalized with respect to the EGFP FIs as an index of protein expression within the cells (left panel in Figure S1b). The normalized NIR FIs of EGFP-expressing cells were only 5 and 3% of those of AR3-EGFP- and Archon1-EGFP-expressing cells, respectively, with red LED (left panel in Figure S1b), indicating that most of the NIR fluorescence signals are attributable to rhodopsins (i.e., AR3 and Archon1). We then evaluated the actual NIR FIs of rhodopsin by subtracting the normalized NIR FIs of EGFP-expressing cells from those of rhodopsin-EGFP-expressing cells (Figure 2c). The rhodopsin FI of Archon1 was larger than that of AR3 as previously reported using the intense laser system.[8] Based on the above results, rhodopsin fluorescence was successfully detected with the low-intensity red LED system.

To investigate the color dependence of FIs of rhodopsins, we imaged rhodopsin-EGFP-expressing cells with green and blue LED stimulation (526 and 477 nm, respectively) (Figures 2b and S1c). As with red LED, little NIR fluorescence signals were observed in EGFP-expressing cells; however, significant signals were observed in AR3-EGFP-expressing and Archon1-

https://doi.org/10.1021/acsomega.2c06980
ACS Omega 2023, 8, 4826−4834

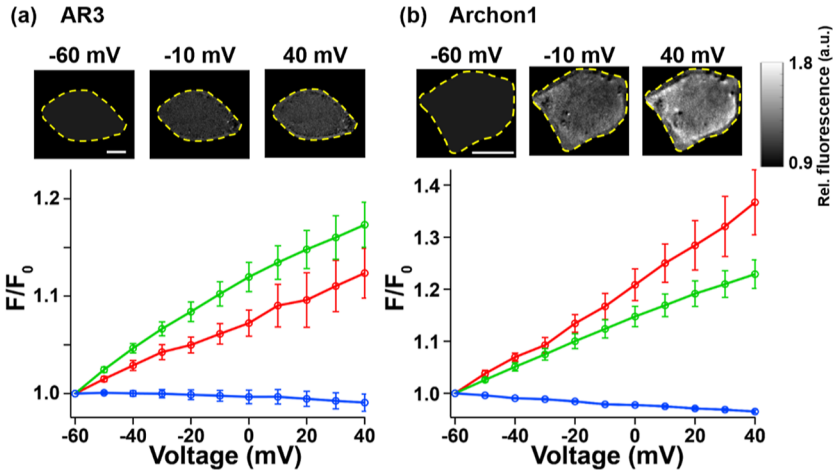

Figure 3. Voltage-dependent changes in the fluorescence of AR3 and Archon1 in HEK293 cells. Voltage-dependent changes in the fluorescence of AR3 (a) and Archon1 (b) in HEK293 cells. The NIR FIs were obtained with red, green, and blue LED stimulation (red, green, and blue circles, respectively). The FIs were normalized at −60 mV. The data are shown as means ± SEM (n = 3−6 cells). (Upper images) NIR fluorescence images of HEK293 cells expressing AR3-EGFP and Archon1-EGFP with green LED stimulation at −60, −10, and 40 mV. Cells are outlined by yellow dashed lines and the outside is painted black. The images were acquired with the oil immersion objective lens (100×/1.3 NA). All scale bars represent 10 μm.

EGFP-expressing cells with green LED (Figure 2b), indicating that most of the observed NIR fluorescence signals were attributed to rhodopsins (middle panel in Figure S1b). The rhodopsin FI of Archon1 was larger than that of AR3 with green and red LEDs (Figure 2c). In contrast, NIR fluorescence signals were clearly observed not only in AR3-EGFP- and Archon1-EGFP-expressing cells but also in EGFP-expressing cells with blue LED (Figure S1c). In fact, the NIR signals of AR3-EGFP- and Archon1-EGFP-expressing cells consisted of signals derived from EGFP by 54 and 73%, respectively (right panel in Figure S1b). Therefore, unlike blue LED, red and green LEDs are effective in selectively detecting rhodopsin fluorescence. The FIs of rhodopsin were plotted against the wavelengths of stimulus light (Figure 2d). The plots were in good agreement with the absorption spectra of AR3 and Archon1. Rhodopsin fluorescence is derived from the three-photon excitation to the initial state, N-intermediate, and Q-intermediate for AR3.[15,16] This suggests that the excitation spectra of rhodopsin fluorescence reflect an integral of the absorption spectra of the three states. The absorption spectra of N- and Q-intermediates are only approximately 10 and 20 nm blue- and red-shifted, respectively, from that of the initial state of AR3.[16] Besides, the fluorescence is proposed to be emitted from the excited state for Archon1. Thus, the excitation spectra of rhodopsin fluorescence are expected to be nearly identical to the absorption spectra of the initial state. In this context, a good agreement between the FIs and absorption spectra suggests that the low-intensity LED system is capable of detecting NIR fluorescence from rhodopsin (Figure 2d).

Next, we investigated the voltage dependence of NIR FIs of AR3 and Archon1 in HEK293 cells. The membrane voltage was varied from −60 to +40 mV with 10 mV changes per step, and NIR fluorescence of AR3-EGFP- and Archon1-EGFP-expressing cells was detected with red, green, and blue LED stimulation (Figures 3 and S2, and Movie S1). The FIs were then plotted against membrane voltage (Figure 3). The changes in fluorescence were dependent on the membrane potential with red and green LEDs but not blue LED. We calculated the ratio of voltage-dependent changes in fluorescence from −60 to +40 mV ($\Delta F/F$) (Table 1). The $\Delta F/F$ values were estimated as 0.12 (red LED) and 0.17 (green LED) for AR3 and 0.36 (red LED) and 0.23 (green LED) for Archon1, while the values for AR3 and Archon1 with blue LED (−0.01 and −0.03, respectively) were nearly zero. The results implied that our observation system efficiently detected the voltage-dependent fluorescence signals of rhodopsin with red and green LEDs. Of note, $\Delta F/F$ values of Archon1 with red and green LEDs (0.36 ± 0.067 and 0.23 ± 0.027) were not significantly different from each other (p > 0.05; Dunnett's test) (Table 1). Considering that the FI of rhodopsin of Archon1 with green LED was 1.5 times larger than that with red LED (Figure 2c and Table 1), we conclude that green LED is as suitable as red LED to monitor the fluorescence of Archon1.

Table 1. NIR FIs and Their Membrane Potential-Dependent Changes in HEK293 Cells[a]

rhodopsin	LED	fluorescence intensity (FI)	fluorescence changes ($\Delta F/F$)
AR3	red	1.0 ± 0.33	0.12 ± 0.030
	green	1.8 ± 0.23	0.17 ± 0.024
	blue	0.85 ± 0.19	−0.01 ± 0.009
Archon1	red	2.0 ± 0.28[b]	0.36 ± 0.067[c]
	green	3.0 ± 0.16[b]	0.23 ± 0.027[c]
	blue	0.84 ± 0.34	−0.03 ± 0.003

[a]Values are shown as mean ± SEM (n = 3−8 cells). [b]Significantly different from each other (p < 0.05; Dunnett's test). [c]Not significantly different from each other (p > 0.05; Dunnett's test).

Applicability of Voltage Imaging System with Low-Intensity LEDs for Different Mammalian Cell Lines. Since we demonstrated the applicability of the low-intensity LED system in detecting rhodopsin fluorescence in HEK293 cells, we further investigated its applicability to other mammalian cell lines using human cervical carcinoma HeLa cells, rat pheochromocytoma PC12 cells, and mouse embryonic carcinoma P19CL6 cells. As in HEK293 cells, NIR fluorescence signal was barely observed for EGFP-expressing

https://doi.org/10.1021/acsomega.2c06980
ACS Omega 2023, 8, 4826−4834

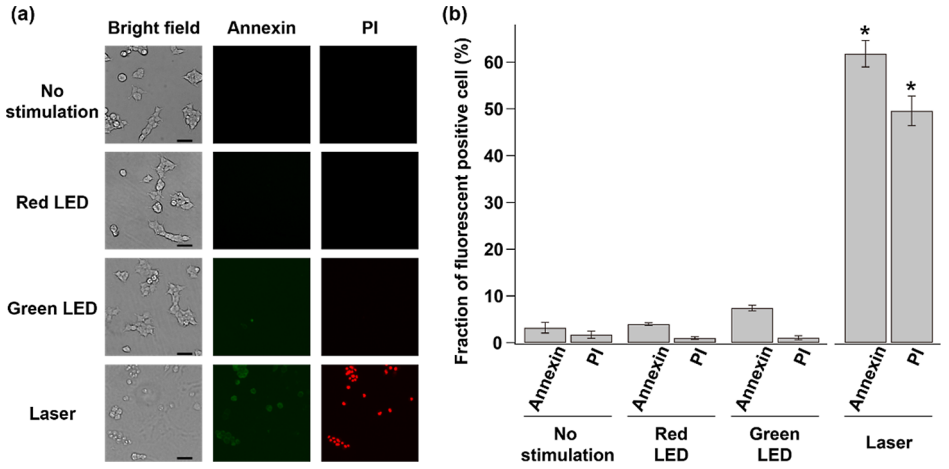

Figure 4. Cell damage after the low-intensity LED stimulation. (a) Bright field and fluorescence images of HEK293 cells stained with Annexin V and PI. Before staining, HEK293 cells were stimulated with red or green LED, high-intensity red laser, or left without stimulation (no stimulation) as a negative control. The images were acquired with the objective lens (10×). All scale bars represent 50 μm. (b) Percentage of Annexin V- and PI-positive cells. The data are shown as means ± SEM (n = 138−1327 cells per dish, n = 3 dishes). Asterisks (*) indicate significant differences from the values without stimulation (p < 0.05; Dunnett's test).

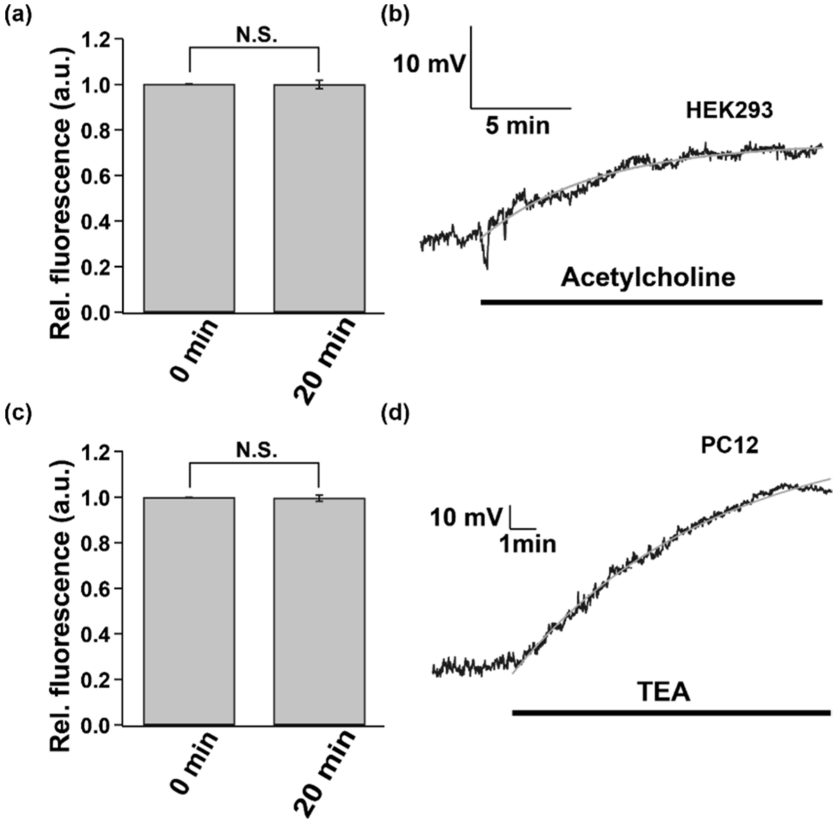

Figure 5. Long-term membrane voltage imaging of HEK293 and PC12 cells. (a,c) Comparison of NIR FIs of Archon1-EGFP-expressing HEK293 (a) and PC12 cells (c) before and after 20 min of imaging with green LED stimulation. The data are shown as means ± SEM (n = 4 cells). N.S. indicates no significant difference (p > 0.05; Student's t-test, two-tailed). (b,d) Voltage imaging of Archon1-EGFP-expressing HEK293 cells treated with acetylcholine (b) and PC12 cells treated with TEA (d). The fitting curves are shown as gray lines.

cells, whereas it was clearly observed for Archon1-EGFP-expressing HeLa, PC12, or P19CL6 cells with green LED (Figure S3). Next, we investigated the voltage-dependence of NIR FIs of Archon1 in these three cell lines (Figure S4). As in HEK293 cells, the FIs increased in a voltage-dependent manner in all three cell lines. These data imply that the low-intensity LED system can detect voltage-dependent fluorescence of rhodopsin in these three mammalian cell lines, which suggests the general applicability of this system for mammalian cells.

Estimation of Cell Damage by Low-Intensity LED Stimulation. High-intensity laser stimulation causes toxicity, lethality, and heat damage in cells and tissues.[18−21] In our observation system, the light intensity of the LED was

https://doi.org/10.1021/acsomega.2c06980
ACS Omega 2023, 8, 4826−4834

suppressed to only 0.15 W/cm^2, which is much lower than that of the intense laser system (1−1000 W/cm^2). Therefore, LED-based system is expected to cause less or no cell damage. HEK293 cells were stimulated with red and green LEDs (0.15 W/cm^2) for 2 h. The cells were then stained with Annexin V and propidium iodide (PI) as apoptosis and cell death markers, respectively, to estimate cell viability (Figure 4a). Annexin V and PI signals were rarely observed in HEK293 cells after red and green LED stimulation as was the case without light stimulation. The percentages of Annexin V- and PI-positive cells after red and green LED stimulation were 4.0 and 1.0 for the red LED and 7.4 and 1.0 for the green LED, respectively, which are similar to those of cells without light stimulation (3.2 and 1.7) (Figure 4b). From these data, we concluded that LED stimulation did not cause significant cell damage. As a control, we also checked Annexin V and PI signals of HEK293 cells after light stimulation with high-intensity red laser pulses (625 nm). The 4 ns pulse laser at 10 Hz was applied to the cells for 8 h, and its average power was adjusted to 1 W/cm^2. Most cells showed Annexin V and PI signals (Figure 4a), and the percentages of Annexin V- and PI-positive cells were 62 and 50, respectively, which are significantly larger than those of cells incubated for 8 h without light stimulation (3.2 and 1.7) (Figure 4b). Therefore, as expected, intense laser stimulation causes severe damage to cells. Based on these results, it can be concluded that the low-intensity LED system is harmless and suitable for long-term imaging. However, it should be noted that the observed severe cell damage is likely due to the high instantaneous intensity of the pulse laser rather than the total optical fluence. Most voltage imaging experiments have been performed with continuous wave (CW) laser and several studies have shown voltage imaging with intense red CW laser stimulation in vivo for tens of minutes with no apparent cell damage.[9,14] Furthermore, laser-induced photochemical toxicity depends on the irradiation wavelength, and the irradiation in the near infrared region (e.g., around 640 nm) exhibits lower toxicity rather than that in shorter wavelength regions (e.g., green and blue).[31] As a future work, we will investigate the cell damage with intense CW laser stimulation instead of the pulse laser and its wavelength dependency.

Long-Term Imaging of Voltage Changes in Drug-Treated Cells with Low-Intensity LED. Since low-intensity LED stimulation did not cause significant damage to cells for 2 h (Figure 4), we examined the applicability of the LED system for long-term imaging. Using a high-intensity laser, the bleaching rate of Archon1 was reported to be 0.01% s^{-1},[8] which implies that the FI of Archon1 decreases by 12% in 20 min. Therefore, high-intensity laser is not suitable for long-term imaging over minutes. To evaluate the bleaching rate of Archon1 in the low-intensity LED system, we continuously imaged the NIR fluorescence of Archon1-EGFP-expressing HEK293 cells with green LED stimulation for 20 min and observed no significant change in FI (Figure 5a). Therefore, the use of low-intensity LED does not induce significant bleaching of fluorescence, which is advantageous for long-term imaging.

Next, we examined the applicability of the LED system for long-term imaging of the slow changes in membrane voltage by continuously imaging the fluorescence of Archon1-EGFP-expressing HEK293 cells treated with acetylcholine for 20 min. Acetylcholine treatment induces slow depolarization (τ = approximately 100 s) of approximately 10 mV through the activation of heterotrimeric G protein.[32] As shown in Figure 3, there is a linear relationship between the FIs and membrane voltage. From this, the FIs were converted into mV based on the $\Delta F/F$ value (i.e., the ratio of voltage-dependent changes in fluorescence from −60 to +40 mV) of Archon1 with green LED. As a results, the resting potential of HEK293 cells was estimated as approximately −50 mV. Then, we observed a slow increase (τ = 340 s) in membrane voltage of 10 mV after acetylcholine treatment (Figure 5b). Therefore, the amplitude and time constant of acetylcholine-induced depolarization were consistent with that in the previous report,[32] indicating that our LED system is capable of detecting drug-induced slow changes in membrane voltage in real-time setting.

We also applied our system to quantitatively assess the kinetics of slow changes in membrane voltage in PC12 cells. Although a K^+ channel blocker, tetraethylammonium chloride (TEA) has been reported to induce depolarization by decreasing the outflow of K^+,[33] and the kinetic parameters (i.e., depolarization amplitude and its time course) remain unknown. Since we confirmed that significant bleaching was not observed in PC12 cells during imaging for 20 min (Figure 5c), we performed continuous fluorescence imaging of Archon1-EGFP-expressing PC12 cells treated with TEA using the LED system. Based on the $\Delta F/F$ value (Figures S4), the resting potential was estimated as approximately −65 mV, and we observed a slow increase (τ = 450 s) in membrane voltage by 50 mV after TEA treatment (Figure 5d). Therefore, the imaging system could quantitatively reveal the kinetic parameters of TEA-induced depolarization. These data demonstrate that the detection system is a promising tool to quantitatively understand the kinetics of slow changes in membrane voltage on long time scales.

In summary, we have developed a new detection system of voltage-dependent rhodopsin fluorescence using a low-intensity LED. Although the time resolution of the LED system is as low as 500 ms at present, the detection system has achieved real-time imaging of drug-induced slow changes in voltage for minutes harmlessly and without fluorescence bleaching. LED excitation is also used for one-photon in vivo wide-field voltage imaging; however, rhodopsin-based GEVIs (e.g., QuasAr2 and Archer1) cannot be applied with the high frame rate (e.g., 30 Hz) due to their dim fluorescence.[34] Since this study demonstrates that the LED system can detect the dim rhodopsin fluorescence with long exposure time (i.e., 500 ms), we speculate that rhodopsin fluorescence can be detected by the one-photon in vivo wide-field voltage imaging using LED with the lower frame rate (e.g., 2 Hz). Very recently, Silapetere et al. detected the rhodopsin fluorescence with fluorescence lifetime imaging microscopy (FLIM) and achieved the imaging of ionophore-induced slow changes in the voltage of *Escherichia coli* cells.[17] Therefore, we propose that our developed detection system is a powerful tool to visualize and quantify slow changes in membrane voltage on long time scales as well as the FLIM method. We expect that the imaging system combining rhodopsin and low-intensity LED will accelerate the quantitative analysis of slow changes in membrane voltage and elucidate their largely unexplored molecular mechanisms during physiological responses and human diseases.[28]

MATERIALS AND METHODS

Gene Construction and Protein Expression in HEK293, HeLa, PC-12, and P19CL6 Cells. The cDNAs for AR3 (Genbank accession number: WP_092921078) and

https://doi.org/10.1021/acsomega.2c06980
ACS Omega 2023, 8, 4826−4834

Archon1 (T20S/G41A/V44E/P60S/T80P/D88N/D95Q/D106H/F161V/A137T/T184I/L199I/G242Q mutant of AR3) (a kind gift from Dr. Edward S Boyden) having optimized codons for the human cells were inserted into the CAG promoter-based mammalian expression vector as previously described.[15] Briefly, EGFP was fused to the C-terminus of each rhodopsin as a reporter. In addition, EGFP was flanked with a membrane trafficking signal motif at the N-terminus and an endoplasmic reticulum export motif at the C-terminus to improve the expression and plasma membrane localization.[35,36]

HEK293T, HeLa, and PC12 cells or P19CL6 cells were cultured in Dulbecco's modified Eagle medium nutrient mixture F-12 (DMEM/F12, Gibco, Thermo Fisher Scientific, USA) or MEM medium (FUJIFILM Wako Pure Chemical Industries, Ltd., Japan) supplemented with 10% fetal bovine serum, 0.0625% (w/v) penicillin, and 0.01% (w/v) streptomycin under a humidified atmosphere containing 5% CO_2 at 37 °C. For rhodopsin expression and fluorescence imaging, the cells were cultured on polylysine-coated glass (Matsunami Glass, Japan). The expression plasmids were transiently transfected using calcium phosphate method into HEK293T and HeLa cells and lipofectamine 3000 (Thermo Fisher Scientific Life Sciences, USA) into PC12 and P19CL6 cells as described elsewhere.[30,37] After 5−6 h of incubation, all-trans retinal (final concentration, 1 μM) was added into the medium for producing the holoprotein (i.e., rhodopsin). After incubation of 12−36 h for HEK293T and P19CL6 cells and 36−48 h for HeLa and PC12 cells, fluorescence images of the cells were obtained.

Fluorescence Imaging of HEK293, HeLa, PC12, and P19CL6 Cells. Fluorescence imaging was performed using an IX73 inverted microscope (Olympus, Japan) at room temperature (approximately 23−28 °C). To observe the NIR fluorescence signals (rhodopsin fluorescence), cell samples were stimulated with red, green, and blue LEDs (050-623, 050-520, and 050-475, respectively, TOFRA, Inc., USA). The peak wavelengths of the stimulus light were set at 624 (red), 526 (green), and 477 (blue) nm using a multiband pass filter (FF01-465/537/623-25, Semrock, USA) and a short-pass filter (SVX630, Asahi Spectra, Japan, <630 nm). The intensity of the stimulus light was adjusted to 0.15 W/cm^2 at the peak wavelengths using an optical power meter (nos. 3664 and 9742, Hioki, Japan). The emitted fluorescence signals through a long-pass filter (FELH0650, THORLABS, USA, >650 nm) were collected using an sCMOS camera (PCO edge 5.5 USB 3.0, PCO., USA). The fluorescence signals for EGFP were observed using the sCMOS camera with excitation at 460−495 nm and emission over 510 nm using a fluorescence mirror unit (U-FBW, Olympus, Japan). Cells were incubated in an extracellular medium (10 mM HEPES, 138 mM NaCl, 3 mM KCl, 1 mM $MgCl_2$, 2 mM $CaCl_2$, and 0.1 M glucose, pH adjusted to 7.3 with NaOH) during imaging. The obtained images were analyzed using ImageJ software (NIH, USA). Membrane regions of the target cells were selected, and the integrated intensities of NIR (rhodopsin fluorescence) and EGFP fluorescence at the membrane were measured separately. The NIR FI was then normalized with respect to the cognate EGFP fluorescence value.[15]

To measure the voltage-dependent changes in fluorescence, imaging was performed under a whole-cell patch-clamp configuration as previously described.[29,30] In brief, the internal pipette solution for whole-cell measurements contained 50 mM HEPES, 140 mM CsCl, 3 mM $MgCl_2$, 5 mM Na_2EGTA, and 2.5 mM MgATP, pH adjusted to 7.3 with CsOH. Cells were incubated in the above extracellular medium, and the membrane voltage of the cells was set from −60 to +40 mV at 10 mV intervals using an EPC 10 USB computer-controlled Patch Clamp amplifier (HEKA Elektronik, Germany) and Patch master software (HEKA Elektronik, Germany).[29,30] The obtained images were analyzed using ImageJ and MATLAB software (Math Works, USA).

Long-Term Fluorescence Imaging of Drug-Treated HEK293 and PC12 Cells. HEK293 and PC12 cells transfected with Archon1 were incubated in the extracellular medium and then treated with acetylcholine (final concentration, 10 μM) and TEA (final concentration, 5 mM), respectively, in fresh medium. The fluorescence images were obtained using a green LED with the same setup as described above. The obtained images were analyzed using ImageJ and MATLAB software. The fluorescence changes were converted into mV based on the $\Delta F/F$ value (i.e., the ratio of voltage-dependent changes in fluorescence from −60 to +40 mV) of Archon1 with green LED (Table 1). Depolarization amplitudes and time constants of HEK293 and PC12 cells were estimated by fitting the time course with a single-exponential function. The data of a previous study[32] were analyzed by WebPlotDigitizer (https://automeris.io/WebPlotDigitizer/) to estimate the depolarization amplitude and time constant.

Protein Purification and Measurement of Absorption Spectra. Recombinant rhodopsin was expressed in *E. coli* cells and purified as previously described.[15,29] The expression plasmids were constructed by inserting cDNA of each rhodopsin into the NdeI and XhoI sites within the multi-cloning site of the expression vectors pKI81 (Novagen, USA) for AR3 and pET21a (+) (Novagen, USA) for Archon1. Recombinant proteins were expressed in *E. coli* BL21 (DE3) and purified by affinity column chromatography as previously described.[15,29] The purified proteins were suspended in a buffer containing 1 M NaCl, 50 mM Tris−HCl, pH 7.0, and 0.05% (w/v) *n*-dodecyl-β-D-maltoside (DDM, Dojindo, Japan), and their absorption spectra were measured using a UV−visible spectrophotometer (UV-2450, Shimadzu, Japan) at room temperature (approximately 23−28 °C).[15]

LED and Laser Irradiation to HEK293 Cells and Analysis of Cell Damage. HEK293 cells were cultured on polylysine-coated glass (Matsunami Glass, Japan) and incubated in CO_2-independent medium (Gibco, Thermo Fisher Scientific Life Sciences, USA) supplemented with 10% fetal bovine serum at room temperature (approximately 23−28 °C). For estimation of cell damage, HEK293 cells were irradiated with red or green LEDs through a multiband pass filter (624 and 526 nm, respectively) as described above. The light intensity was adjusted to 0.15 W/cm^2 at the peak wavelengths, and the cells were continuously stimulated for 2 h. To assess the effect of laser irradiation on HEK293 cells, the cells were irradiated with laser pulses (Nd/YAG laser, Surelite I-10, Continuum, USA). The wavelength of the laser was tuned at 625 nm (4 ns) using an optical parametric oscillator (Surelite OPO Plus, Continuum, USA).[29,30] The average intensity of the stimulus light was adjusted to 1 W/cm^2. The 4 ns pulse laser at 10 Hz was applied to the cells for 8 h (total irradiation time = 1.152 ms). As a negative control, HEK293 cells were incubated in a CO_2-independent medium without light stimulation for 8 h. Cellular apoptosis was measured using the Annexin V-633 apoptosis detection kit (Nacalai Tesque,

https://doi.org/10.1021/acsomega.2c06980
ACS Omega 2023, 8, 4826−4834

Japan) as previously described.[38] Cells were washed with phosphate-buffered saline and incubated in a reaction buffer containing Annexin V-633 and PI according to the manufacturer's instructions.[38] Fluorescence signals for Annexin V and PI were observed using an IX71 inverted microscope (Olympus, Japan) equipped with a CCD camera (ORCA-AG, Hamamatsu, Japan). Annexin V was stimulated at 640 ± 10 nm, and fluorescence signals were collected through a long-pass filter (>695 nm). PI was stimulated at 540 ± 10 nm, and fluorescence signals were collected at 620 ± 10 nm. The obtained images were analyzed using ImageJ software.

■ ASSOCIATED CONTENT

Supporting Information

The Supporting Information is available free of charge at https://pubs.acs.org/doi/10.1021/acsomega.2c06980.

Gene construction, bright field and fluorescence images of mammalian cells, NIR FI of mammalian cells, and voltage-dependent fluorescence changes of AR3 and Archon1 (PDF)

Voltage-dependent fluorescence changes of AR3 and Archon1 in HEK293 cells (AVI)

■ AUTHOR INFORMATION

Corresponding Authors

Keiichi Kojima − *Graduate School of Medicine, Dentistry and Pharmaceutical Sciences and Faculty of Medicine, Dentistry and Pharmaceutical Sciences, Okayama University, Okayama 700-8530, Japan;* orcid.org/0000-0003-4729-0511; Phone: +81-86-251-7980; Email: keiichikojima@okayama-u.ac.jp

Yuki Sudo − *Graduate School of Medicine, Dentistry and Pharmaceutical Sciences and Faculty of Medicine, Dentistry and Pharmaceutical Sciences, Okayama University, Okayama 700-8530, Japan;* orcid.org/0000-0001-8155-9356; Phone: +81-86-251-7945; Email: sudo@okayama-u.ac.jp

Authors

Shiho Kawanishi − *Graduate School of Medicine, Dentistry and Pharmaceutical Sciences, Okayama University, Okayama 700-8530, Japan*

Atsushi Shibukawa − *Graduate School of Medicine, Dentistry and Pharmaceutical Sciences, Okayama University, Okayama 700-8530, Japan;* Present Address: Research Institute for Electronic Science, Hokkaido University, Kita 21 Nishi 10, Kita-ku, Sapporo, Hokkaido 001-0021, Japan

Masayuki Sakamoto − *Department of Optical Neural and Molecular Physiology, Graduate School of Biostudies, Kyoto University, Kyoto 606-8507, Japan*

Complete contact information is available at: https://pubs.acs.org/10.1021/acsomega.2c06980

Author Contributions

The manuscript was written through contributions of all authors. All authors have given approval to the final version of the manuscript.

Funding

This work was financially supported by JSPS KAKENHI grant numbers JP19K16090 and JP21K15054 to KK and JP18H02411, JP19H04727, JP19H05396, and JP20K21482 to YS. This research was partially supported by Precursory Research for Embryonic Science and Technology (PRESTO) and AMED (JP20dm0207101) to MS and JST-CREST (JPMJCR1656) and AMED (JP20dm0207060) to YS.

Notes

The authors declare no competing financial interest.

■ ACKNOWLEDGMENTS

We wish to thank Dr. Edward S Boyden for providing the Archon1 gene. We also wish to thank "Editage" (http://www.editage.com) for the English language review.

■ REFERENCES

(1) Ernst, O. P.; Lodowski, D. T.; Elstner, M.; Hegemann, P.; Brown, L. S.; Kandori, H. Microbial and animal rhodopsins: structures, functions, and molecular mechanisms. *Chem. Rev.* **2014**, *114*, 126−163.

(2) Govorunova, E. G.; Sineshchekov, O. A.; Li, H.; Spudich, J. L. Microbial rhodopsins: diversity, mechanisms, and optogenetic applications. *Annu. Rev. Biochem.* **2017**, *86*, 845−872.

(3) Kojima, K.; Shibukawa, A.; Sudo, Y. The unlimited potential of microbial rhodopsins as optical tools. *Biochemistry* **2020**, *59*, 218−229.

(4) Kralj, J. M.; Douglass, A. D.; Hochbaum, D. R.; Maclaurin, D.; Cohen, A. E. Optical recording of action potentials in mammalian neurons using a microbial rhodopsin. *Nat. Methods* **2011**, *9*, 90−95.

(5) Ihara, K.; Umemura, T.; Katagiri, I.; Kitajima-Ihara, T.; Sugiyama, Y.; Kimura, Y.; Mukohata, Y. Evolution of the archaeal rhodopsins: evolution rate changes by gene duplication and functional differentiation. *J. Mol. Biol.* **1999**, *285*, 163−174.

(6) Xu, Y.; Zou, P.; Cohen, A. E. Voltage imaging with genetically encoded indicators. *Curr. Opin. Chem. Biol.* **2017**, *39*, 1−10.

(7) Hochbaum, D. R.; Zhao, Y.; Farhi, S. L.; Klapoetke, N.; Werley, C. A.; Kapoor, V.; Zou, P.; Kralj, J. M.; Maclaurin, D.; Smedemark-Margulies, N.; Saulnier, J. L.; Boulting, G. L.; Straub, C.; Cho, Y. K.; Melkonian, M.; Wong, G. K.; Harrison, D. J.; Murthy, V. N.; Sabatini, B. L.; Boyden, E. S.; Campbell, R. E.; Cohen, A. E. All-optical electrophysiology in mammalian neurons using engineered microbial rhodopsins. *Nat. Methods* **2014**, *11*, 825−833.

(8) Piatkevich, K. D.; Jung, E. E.; Straub, C.; Linghu, C.; Park, D.; Suk, H. J.; Hochbaum, D. R.; Goodwin, D.; Pnevmatikakis, E.; Pak, N.; Kawashima, T.; Yang, C. T.; Rhoades, J. L.; Shemesh, O.; Asano, S.; Yoon, Y. G.; Freifeld, L.; Saulnier, J. L.; Riegler, C.; Engert, F.; Hughes, T.; Drobizhev, M.; Szabo, B.; Ahrens, M. B.; Flavell, S. W.; Sabatini, B. L.; Boyden, E. S. A robotic multidimensional directed evolution approach applied to fluorescent voltage reporters. *Nat. Chem. Biol.* **2018**, *14*, 352−360.

(9) Adam, Y.; Kim, J. J.; Lou, S.; Zhao, Y.; Xie, M. E.; Brinks, D.; Wu, H.; Mostajo-Radji, M. A.; Kheifets, S.; Parot, V.; Chettih, S.; Williams, K. J.; Gmeiner, B.; Farhi, S. L.; Madisen, L.; Buchanan, E. K.; Kinsella, I.; Zhou, D.; Paninski, L.; Harvey, C. D.; Zeng, H.; Arlotta, P.; Campbell, R. E.; Cohen, A. E. Voltage imaging and optogenetics reveal behaviour-dependent changes in hippocampal dynamics. *Nature* **2019**, *569*, 413−417.

(10) Chien, M. P.; Brinks, D.; Testa-Silva, G.; Tian, H.; Phil Brooks, F., 3rd; Adam, Y.; Bloxham, B.; Gmeiner, B.; Kheifets, S.; Cohen, A. E. Photoactivated voltage imaging in tissue with an archaerhodopsin-derived reporter. *Sci. Adv.* **2021**, *7*, No. eabe3216.

(11) Tian, H.; Davis, H. C.; Wong-Campos, J. D.; Fan, L. Z.; Gmeiner, B.; Begum, S.; Werley, C. A.; Borja, G. B.; Upadhyay, H.; Shah, H.; Jacques, J.; Park, P.; Qi, Y.; Parot, V.; Deisseroth, K.; Cohen, A. E. All-optical electrophysiology with improved genetically encoded voltage indicators reveals interneuron network dynamics in vivo. *Nat. Methods* **2021**, DOI: 10.1038/s41592-022-01743-5.

(12) Bando, Y.; Grimm, C.; Cornejo, V. H.; Yuste, R. Genetic voltage indicators. *BMC Biol.* **2019**, *17*, 71.

(13) Zhang, X. M.; Yokoyama, T.; Sakamoto, M. Imaging voltage with microbial rhodopsins. *Front. Mol. Biosci.* **2021**, *8*, 738829.

(14) Fan, L. Z.; Kheifets, S.; Böhm, U. L.; Wu, H.; Piatkevich, K. D.; Xie, M. E.; Parot, V.; Ha, Y.; Evans, K. E.; Boyden, E. S.; Takesian, A. E.; Cohen, A. E. All-optical electrophysiology reveals the role of lateral inhibition in sensory processing in cortical layer 1. *Cell* **2020**, *180*, 521−535.
(15) Kojima, K.; Kurihara, R.; Sakamoto, M.; Takanashi, T.; Kuramochi, H.; Zhang, X. M.; Bito, H.; Tahara, T.; Sudo, Y. Comparative studies of the fluorescence properties of microbial rhodopsins: spontaneous emission versus photointermediate fluorescence. *J. Phys. Chem. B* **2020**, *124*, 7361−7367.
(16) Maclaurin, D.; Venkatachalam, V.; Lee, H.; Cohen, A. E. Mechanism of voltage-sensitive fluorescence in a microbial rhodopsin. *Proc. Natl. Acad. Sci. U.S.A.* **2013**, *110*, 5939−5944.
(17) Silapetere, A.; Hwang, S.; Hontani, Y.; Fernandez Lahore, R. G.; Balke, J.; Escobar, F. V.; Tros, M.; Konold, P. E.; Matis, R.; Croce, R.; Walla, P. J.; Hildebrandt, P.; Alexiev, U.; Kennis, J. T. M.; Sun, H.; Utesch, T.; Hegemann, P. QuasAr Odyssey: the origin of fluorescence and its voltage sensitivity in microbial rhodopsins. *Nat. Commun.* **2022**, *13*, 5501.
(18) Thomsen, S. Pathologic analysis of photothermal and photomechanical effects of laser-tissue interactions. *Photochem. Photobiol.* **1991**, *53*, 825−835.
(19) Hawkins, D. H.; Abrahamse, H. The role of laser fluence in cell viability, proliferation, and membrane integrity of wounded human skin fibroblasts following helium-neon laser irradiation. *Lasers Surg. Med.* **2006**, *38*, 74−83.
(20) Silva, I. H.; de Andrade, S. C.; de Faria, A. B.; Fonsêca, D. D.; Gueiros, L. A.; Carvalho, A. A.; da Silva, W. T.; de Castro, R. M.; Leão, J. C. Increase in the nitric oxide release without changes in cell viability of macrophages after laser therapy with 660 and 808 nm lasers. *Laser Med. Sci.* **2016**, *31*, 1855−1862.
(21) Arias-Gil, G.; Ohl, F. W.; Takagaki, K.; Lippert, M. T. Measurement, modeling, and prediction of temperature rise due to optogenetic brain stimulation. *Neurophotonics* **2016**, *3*, 045007.
(22) Baczkó, I.; Giles, W. R.; Light, P. E. Pharmacological activation of plasma-membrane KATP channels reduces reoxygenation-induced Ca^{2+} overload in cardiac myocytes via modulation of the diastolic membrane potential. *Br. J. Pharmacol.* **2004**, *141*, 1059−1067.
(23) Chilton, L.; Ohya, S.; Freed, D.; George, E.; Drobic, V.; Shibukawa, Y.; MacCannell, K. A.; Imaizumi, Y.; Clark, R. B.; Dixon, I. M.; Giles, W. R. K^+ currents regulate the resting membrane potential, proliferation, and contractile responses in ventricular fibroblasts and myofibroblasts. *Am. J. Physiol.: Heart Circ. Physiol.* **2005**, *288*, H2931−H2939.
(24) Langheinrich, U.; Daut, J. Hyperpolarization of isolated capillaries from guinea-pig heart induced by K^+ channel openers and glucose deprivation. *J. Physiol.* **1997**, *502*, 397−408.
(25) Onohara, N.; Nishida, M.; Inoue, R.; Kobayashi, H.; Sumimoto, H.; Sato, Y.; Mori, Y.; Nagao, T.; Kurose, H. TRPC3 and TRPC6 are essential for angiotensin II-induced cardiac hypertrophy. *EMBO J.* **2006**, *25*, 5305−5316.
(26) Franco, R.; Bortner, C. D.; Cidlowski, J. A. Potential roles of electrogenic ion transport and plasma membrane depolarization in apoptosis. *J. Membr. Biol.* **2006**, *209*, 43−58.
(27) Sundelacruz, S.; Levin, M.; Kaplan, D. L. Role of membrane potential in the regulation of cell proliferation and differentiation. *Stem Cell Rev. Rep.* **2009**, *5*, 231−246.
(28) Abdul Kadir, L.; Stacey, M.; Barrett-Jolley, R. Emerging roles of the membrane potential: Action beyond the action potential. *Front. Physiol.* **2018**, *9*, 1661.
(29) Kikuchi, M.; Kojima, K.; Nakao, S.; Yoshizawa, S.; Kawanishi, S.; Shibukawa, A.; Kikukawa, T.; Sudo, Y. Functional expression of the eukaryotic proton pump rhodopsin *Om*R2 in *Escherichia coli* and its photochemical characterization. *Sci. Rep.* **2021**, *11*, 14765.
(30) Kojima, K.; Miyoshi, N.; Shibukawa, A.; Chowdhury, S.; Tsujimura, M.; Noji, T.; Ishikita, H.; Yamanaka, A.; Sudo, Y. Green-sensitive, long-lived, step-functional anion channelrhodopsin-2 variant as a high-potential neural silencing tool. *J. Phys. Chem. Lett.* **2020**, *11*, 6214−6218.
(31) Wäldchen, S.; Lehmann, J.; Klein, T.; van de Linde, S.; Sauer, M. Light-induced cell damage in live-cell super-resolution microscopy. *Sci. Rep.* **2015**, *5*, 15348.
(32) Yamada, A.; Gaja, N.; Ohya, S.; Muraki, K.; Narita, H.; Ohwada, T.; Imaizumi, Y. Usefulness and limitation of $DiBAC_4(3)$, a voltage-sensitive fluorescent dye, for the measurement of membrane potentials regulated by recombinant large conductance Ca^{2+}-activated K^+ channels in HEK293 cells. *Jpn. J. Pharmacol.* **2001**, *86*, 342−350.
(33) Huang, C. L.; Chen, H. C.; Huang, N. K.; Yang, D. M.; Kao, L. S.; Chen, J. C.; Lai, H. L.; Chern, Y. Modulation of dopamine transporter activity by nicotinic acetylcholine receptors and membrane depolarization in rat pheochromocytoma PC12 cells. *J. Neurochem.* **1999**, *72*, 2437−2444.
(34) Bando, Y.; Sakamoto, M.; Kim, S.; Ayzenshtat, I.; Yuste, R. Comparative evaluation of genetically encoded voltage indicators. *Cell Rep.* **2019**, *26*, 802.
(35) Gradinaru, V.; Thompson, K. R.; Deisseroth, K. eNpHR: a Natronomonas halorhodopsin enhanced for optogenetic applications. *Brain Cell Biol.* **2008**, *36*, 129−139.
(36) Gradinaru, V.; Zhang, F.; Ramakrishnan, C.; Mattis, J.; Prakash, R.; Diester, I.; Goshen, I.; Thompson, K. R.; Deisseroth, K. Molecular and cellular approaches for diversifying and extending optogenetics. *Cell* **2010**, *141*, 154−165.
(37) Kojima, K.; Yamashita, T.; Imamoto, Y.; Kusakabe, T. G.; Tsuda, M.; Shichida, Y. Evolutionary steps involving counterion displacement in a tunicate opsin. *Proc. Natl. Acad. Sci. U.S.A.* **2017**, *114*, 6028−6033.
(38) Nakao, S.; Kojima, K.; Sudo, Y. Phototriggered apoptotic cell death (PTA) using the light-driven outward proton pump rhodopsin Archaerhodopsin-3. *J. Am. Chem. Soc.* **2022**, *144*, 3771−3775.

https://doi.org/10.1021/acsomega.2c06980
ACS Omega 2023, 8, 4826−4834